

Gold catalyzed growth of silicon nanowires by plasma enhanced chemical vapor deposition

S. Hofmann,^{a)} C. Ducati, R. J. Neill, S. Piscanec, and A. C. Ferrari
Department of Engineering, University of Cambridge, Cambridge CB2 1PZ, United Kingdom

J. Geng
Department of Chemistry, University of Cambridge, Cambridge CB2 1EW, United Kingdom

R. E. Dunin-Borkowski
Department of Materials Science and Metallurgy, University of Cambridge, Cambridge CB2 3QZ, United Kingdom

J. Robertson
Department of Engineering, University of Cambridge, Cambridge CB2 1PZ, United Kingdom

(Received 7 April 2003; accepted 7 August 2003)

Silicon nanowires were selectively grown at temperatures below 400 °C by plasma enhanced chemical vapor deposition using silane as the Si source and gold as the catalyst. A detailed growth study is presented using electron microscopy, focused ion beam preparation, and Raman spectroscopy. A radio-frequency plasma significantly increased the growth rate. The Si nanowires show an uncontaminated, crystalline silicon core surrounded by a 2-nm-thick oxide sheath. The as-grown diameters are small enough for the observation of quantum confinement effects. Plasma activation could allow a further decrease in deposition temperature. A growth model for plasma enhanced nanowire growth is discussed. © 2003 American Institute of Physics.
[DOI: 10.1063/1.1614432]

I. INTRODUCTION

Crystalline nanostructures such as nanotubes and nanowires offer unique access to low-dimensional physics, and they can be used as nanotechnology building blocks to reach higher device integration densities than conventional fabrication methods.^{1,2} A great advantage of synthetic nanocrystals is that they inherently grow in nanometer size, without the need of complicated lithography processes. One-dimensional nanomaterials could play a key role in nanotechnology, as well as provide model systems to demonstrate quantum size effects. However, their small size makes the assembly and integration difficult, so nanostructures will not realize their full potential until their growth can be controlled accurately.

Nanowires have recently attracted attention as an alternative system to carbon nanotubes (CNTs).³ The extensive study of CNTs in the past decade has hit problems, some of which might be overcome by using nanowires.³ Silicon nanowires (SiNWs) are particularly attractive due to the central role of the silicon semiconductor industry, which would allow Si nanowires to be implemented using existing technologies. The bulk properties of silicon are well understood. Therefore, SiNWs offer an ideal basis to study the effects of quantum confinement and possible applications. The carrier type and concentration in crystalline SiNWs could be controlled by doping, as in bulk Si.⁴ Silicon turns into a direct band-gap semiconductor at nanometer size due to quantum confinement,^{5,6} so it could be used in optoelectronics, unlike bulk Si.

Different methods have been used to synthesize SiNWs: chemical vapor deposition (CVD),⁷ laser-ablation,⁸ evaporation,⁹ and solution-based methods.¹⁰ Various directional features of these techniques were reported and a model proposed for preferred SiNW growth directions.¹¹ High-temperature laser ablation enables metal-catalyst-free growth based on SiO₂ assisted synthesis.¹² CVD does require the use of a metal catalyst, but this allows controlled, selective growth by pre patterning the metal on the substrate. This method is often based on the vapor-liquid-solid (VLS) idea¹³ in which various metals, such as Au,^{7,13} Fe,^{8,14} Ti,¹⁵ and Ga,¹⁶ catalytically enhance the growth of SiNWs. Ga appears to be the most favorable catalyst for low-temperature synthesis from its phase diagram, because the Ga-Si system has a very low eutectic temperature.¹⁶ However, the diffusivity and possible contamination by the catalyst makes Ga less favored, and Ti a more promising catalyst.¹⁵

We used Au as a catalyst, as it does not form a silicide and the bulk Au/Si eutectic temperature is relatively low (363 °C) compared to other catalysts, like Fe and Ti. Hence, Au gives low-temperature growth but it does not leave a fast diffusing impurity.

In this article, we demonstrate the selective growth of SiNWs at temperatures below 400 °C. This is achieved by using a commercial plasma enhanced chemical vapor deposition (PECVD) system typically used to grow silicon thin films.

The ability to grow at low temperatures is important for device integration. We show that a low-power radio frequency (rf) plasma significantly increases the growth rate, without decreasing the high crystallinity of the as-grown

^{a)}Electronic mail: sh315@eng.cam.ac.uk

structures. As in carbon nanotubes, plasma enhancement may allow the growth of SiNWs at lower substrate temperatures.^{17,18} For example, a microwave plasma gave SiNWs without needing a separate heater.¹⁶

Focusing on the influence of the Au catalyst, we present a detailed electron microscopy study comparing the use of different Au film thicknesses and Au colloidal suspensions. Quantum confinement was recently demonstrated in SiNWs by scanning tunneling microscopy on single, oxide-removed SiNWs.¹⁹ Here, we show that Raman spectroscopy is a simple way to demonstrate phonon confinement effects. This also allows us to probe quickly and nondestructively the average diameter of SiNWs. Finally, we discuss possible growth mechanisms for PECVD and thermally grown SiNWs.

II. EXPERIMENTAL DETAILS

A 20-nm-thick SiO₂ layer was grown by thermal oxidation or low-temperature electron cyclotron resonance (ECR) onto polished *n*-type Si(100) substrates to act as a catalyst diffusion barrier. Au was deposited by evaporating Au metal (99.99%) from a tungsten boat in a standard evaporator at a base pressure below 10⁻⁶ mbar. The thickness of the Au layer was determined by profilometry and conductivity measurements. Au colloidal suspensions were made by the reduction of aqueous HAuCl₄ solution by sodium citrate at 110 °C.²⁰ The resulting Au suspension has clusters of Au with diameter 16 nm ± 10% and contains 5.8 mg of Au per 100 ml H₂O. The colloids can be applied directly or with the help of a surfactant on the substrates.

The samples were then loaded into the rf parallel plate PECVD system (Plasmalab DP 80). Typically, between 10 and 20 samples were loaded at the same time. The samples were heated to 380 °C under vacuum, and allowed to outgas for 3 h. The process gases were then admitted at various flow rates. The gas flow was maintained for between 15 and 90 min and pressures between 0.4 and 2.4 mbar. 13.6 MHz rf power was supplied to create a plasma, except when a thermal reaction was desired.

The structure and composition of the SiNWs were analyzed by a combination of scanning electron microscopy (SEM) (Jeol 6340 FEGSEM), high-resolution transmission electron microscopy (HRTEM) (Jeol JEM 4000EX, 400 kV), energy-dispersive x-ray spectroscopy (EDX), electron energy loss spectroscopy (EELS) [Philips CM300ST with Gatan imaging filter (GIF) 2000] and Raman spectroscopy (Renishaw MicroRaman 1000, 514.5 nm Ar-ion laser). For HRTEM, EDX, and EELS analyses, the as-grown samples were removed from the substrates and dispersed onto 1000 mesh Au grids, Cu finder grids, or lacey carbon grids. Pt contacts for pinning individual SiNWs and trench markers were deposited or milled on the samples by a focused ion beam (FIB) (FEI 200FX).

III. RESULTS AND DISCUSSION

In order to observe quantum confinement effects, the nanowire core diameter must be reduced to 10 nm or less. Using silane as the Si source gas allows growth of smaller

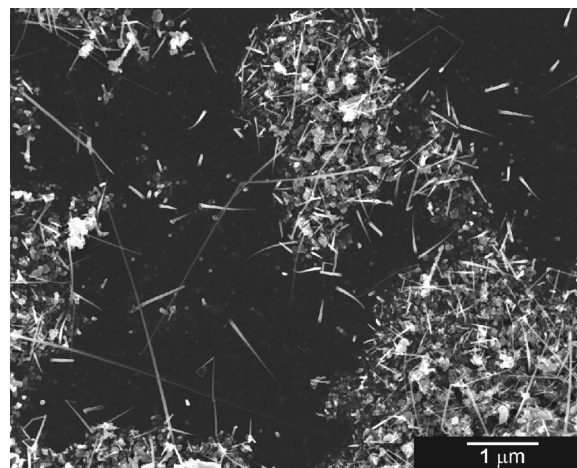


FIG. 1. SEM photograph of Si nanostructures grown at 0.4 mbar, 380 °C, and 10 W rf power for 15 min.

diameter SiNWs and lower growth temperatures compared to SiCl₄.⁷ It is also known that a higher SiH₄ partial pressure gives smaller diameter SiNWs.⁷ Therefore, we used undiluted silane as the precursor gas.

The SiNW growth rate was about 0.2 nm s⁻¹ at a silane pressure of 0.4 mbar at 380 °C without a plasma. A gold catalyst layer of more than 3 nm thickness showed no nanowire growth at these conditions.

To increase the growth rate, a 13.6 MHz rf plasma was then used. Figure 1 shows a SEM image of Si nanostructures grown at 0.4 mbar, 380 °C, and 10 W rf power for 15 min. The initial 3-nm-thick Au catalyst layer formed droplets with an average diameter below 30 nm. The nanowires originate from those droplets, adopting the size of the initial Au nuclei. However, a large fraction of the Au catalyst did not nucleate any structure and is aggregated. The nanowires are typically less than 2 μm long and slightly tapered, with a smaller diameter at the tip than at the bottom. The taper was also reported for Ti-catalyzed SiNWs,²¹ and it can be attributed to the uncatalyzed deposition of Si on the sides of wires during growth.

The unwanted uncatalyzed Si deposition and catalyzed SiNW growth always coexist. A key role of Au is to make the catalytic process dominant under given conditions. Note that low growth temperature enhances the controlled catalytic nanowire growth by thermal CVD, as it has a lower activation energy than uncatalyzed Si deposition.²²

Rather than selectively increasing the nanowire (NW) growth rate, an applied rf plasma also enhances the uncatalyzed decomposition of the Si precursor gas. A large rf power, therefore, causes the Au catalyst to become covered with *a*-Si and deactivated. A 3 nm Au film did hardly nucleate any nanowire in a 100 W plasma, and gave only a rough surface, indicating coverage by *a*-Si. In order to use a higher plasma power for higher plasma activation, the silane must be diluted by an etchant such as hydrogen. This is similar to the PECVD of carbon nanotubes, where an etchant gas is used to minimize uncatalyzed surface deposition.²³ We are presently investigating the effect of rf power on SiNW growth to reduce the substrate temperature.^{17,18} This could allow direct growth of SiNWs onto low-temperature sub-

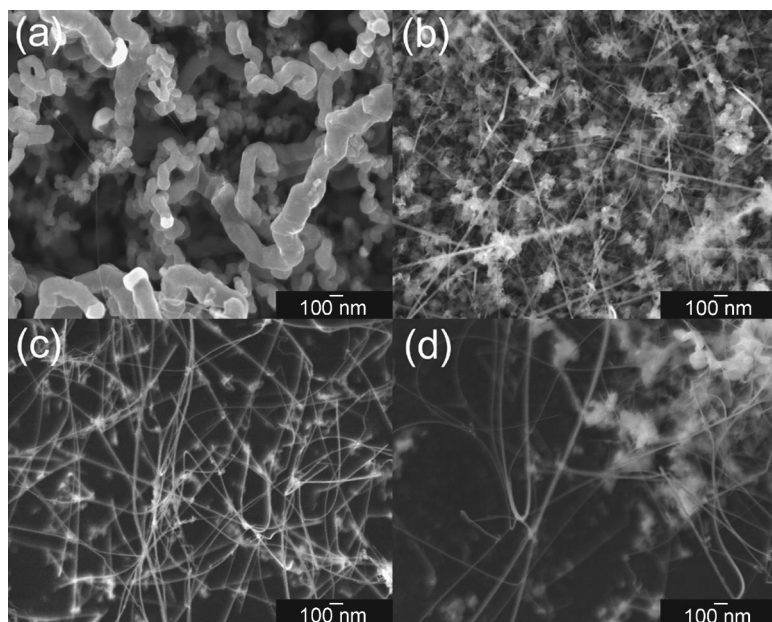


FIG. 2. SEM photographs of SiNWs grown at 2 mbar, 380 °C, and 10 W rf power for 90 min from evaporated Au thin films of decreasing thickness [(a): 5 nm, (b): 1 nm, (c): 0.5 nm] and a Au colloidal suspension (d).

strates and allow their integration in sensitive nanoelectronic devices.

Figure 2 shows SEM images of samples processed at 2 mbar, 380 °C, and 10 W rf power for 90 min. A higher silane pressure gives a higher catalytical growth rate. The nanowires are not tapered. Figures 2(a)–2(c) show the effect of the Au film thickness on growth. In Fig. 2(a), a 5-nm-thick Au film creates worm-like structures of up to 300 nm in diameter. A Au droplet of similar diameter can be seen on the tip of the structures indicating catalytical growth. In addition, very straight, small diameter (<15 nm) wires are found. In Fig. 2(b), a 1-nm-thick Au film gives both long straight wires and worm-like structures. The straight wires are now more abundant, and the worm-like structures have a smaller diameter (<100 nm) than in Fig. 2(a). In Fig. 2(c), for an Au thickness of ~ 0.5 nm, the total yield is lower and the sub-

strate is seen in the background. The SEM image allows no structural distinction, as all the structures have small diameters (<20 nm) and are mainly straight.

Figure 2(d) shows SiNWs grown from a colloidal Au suspension. As in previous reports,²⁴ the SiNWs have diameters slightly larger than the colloidal diameter of 16 nm. Despite an initial homogenous dispersion on the substrate, the Au colloids do agglomerate, leading to a larger diameter distribution and to some worm-like features similar to Fig. 2(b). The synthesis method for the colloidal gold sol allows smaller initial diameters.²⁰ Here the similarity to the evaporated Au film is emphasized.

HRTEM supports the structural distinction made above. For all deposition conditions, straight nanowires are highly crystalline, whereas worm-like structures are amorphous [Figs. 3(a)–3(c), and 3(d), respectively]. The growth direc-

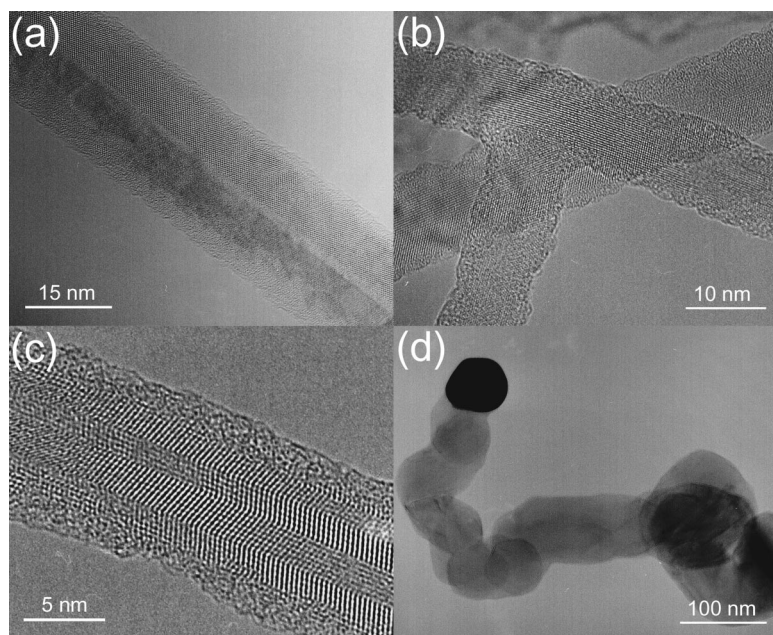


FIG. 3. HRTEM images of as-grown nanowires. A structural distinction between straight, crystalline SiNWs [(a)–(c)] and amorphous, worm-like structures (d) can be made.

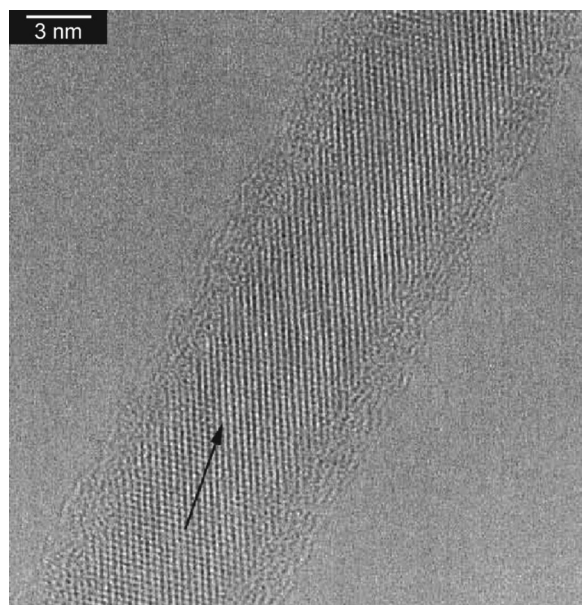


FIG. 4. HRTEM image of a portion of a nanowire taken along the [011] direction. A well-crystallized core of 7.2 nm and an amorphous outer layer 1.5–1.7 nm thick can be seen. The wire axis lies at about 12° to the [11-1] direction, as indicated.

tion of many SiNWs is found to be [110] from analysis of the lattice fringes. However, wires with other growth directions are also observed. Figures 3–6 show the samples of Fig. 2 dispersed on transmission electron microscopy (TEM) grids. Figures 3(a) and 3(c) show HRTEM images of Si nanowires taken along the [110] direction. The nanowire in Fig. 3(a) has a crystalline core of about 17 nm diameter, and an amorphous shell of 2 nm. Different sets of crystallographic planes can be identified, corresponding to the {111}, {002}, and {220} planes (interplanar distances of 3.14, 2.71, and 1.92 Å, respectively). The growth direction is the [2-20] direction. Figure 3(c), a close up of Fig. 3(b), shows the nanowire to consist of a crystalline core 7.4 nm in diameter covered by a 1.5–2 nm amorphous layer. The lattice fringes parallel to the wire axis correspond to the (1-1-1) planes, and hence, its growth direction is [1-12]. The four bands lying along the [1-12] direction are due to twins on the (1-1-1) planes.

Figure 4 shows a SiNW about 10.3 nm in diameter, with a well-crystallized core of 7.2 nm and an amorphous outer layer 1.5–1.7 nm in thickness. The image was taken along the [011] direction. The lattice fringes correspond to the (11-1), (1-11), and (200) planes, with spacings of 3.14 and 2.71 Å, respectively. The wire axis does not correspond to a specific crystallographic direction, but lies at about 12° to [11-1], as indicated in Fig. 4.

Most nanowires (>70%) show no catalyst particle at their tip, which suggests a base growth mechanism. Some SiNWs, however, have a Au particle at the tip, which seems to determine the diameter of the structure. In particular, the wires with kinks, such as in Fig. 5, have a Au particle at the tip [Fig. 5(a)].

Although most of the nanowires are straight, kinking can be observed (Fig. 5). Reflecting the high crystallinity, kinking at sharp angles is seen, [Fig. 5(b)]. Kinking may be re-

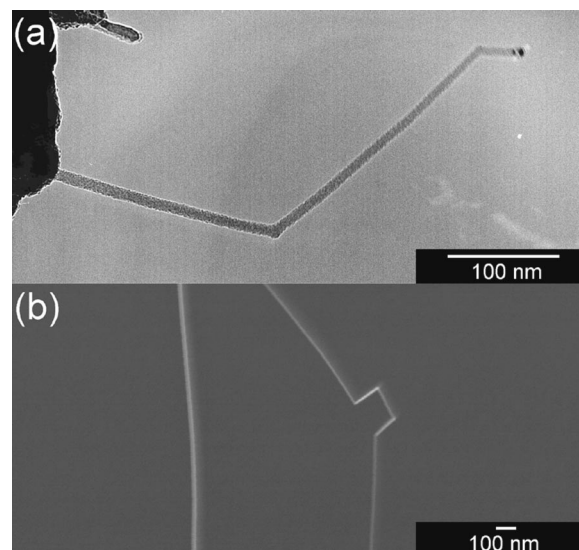


FIG. 5. (a) TEM and (b) SEM image of growth defects (kinks).

lated to growth defects and high growth rates.⁷

The worm-like structures have a diameter of 80–300 nm, which is not uniform along the wire length. Figure 3(d) shows that the worm-like wires are randomly oriented, with a rapidly varying growth direction. The TEM contrast shows that these structures are amorphous, with small isolated crystalline inclusions. A spherical gold particle was always found at the tip of the amorphous wires.

Figure 6 shows the results of EELS elemental mapping of part of a 14-nm-diameter crystalline nanowire. The analysis was performed in a field emission gun TEM operated at 300 kV. The bright-field image [Fig. 6(a)] was acquired slightly underfocus. Three-window background-subtracted elemental maps were acquired using the oxygen *K* edge (532 eV) [Fig. 6(b)] and the Si *K* edge (1839 eV) [Fig. 6(c)] on a 2048×2048 pixel charge-coupled-device (CCD) camera. The chemical maps represent the projected elemental concentrations in the electron beam direction. The analysis shows a silicon core surrounded by an approximately 2-nm-thick SiO_x sheath. This is consistent with the outer 2 nm amorphous layers seen in the HRTEM images above (Figs. 3 and 4). The SiO_x layer is most likely native silicon oxide formed during extended air exposure after deposition.

Energy dispersive x-ray spectroscopy was performed as well as EELS to test for possible contamination in the as-grown SiNWs. No elements other than Si and O could be traced along the nanowires within the sensitivity of the method. Au could only be found at the base and sometimes at the tip of the SiNWs, as described in the HRTEM analysis. It should be emphasized that the measured purity is not self-evident and accidental impurities can be found.¹⁴ This confirms that Au is a suitable catalyst material for the conditions used.

CVD allows selective growth, unlike other methods such as laser ablation.^{8,14} This is important not only for applications but also for further characterization. Figure 7(a) shows as-grown SiNWs from a patterned 1-nm-thick Au layer. The evaporated Au was patterned using a 2000 mesh Cu TEM

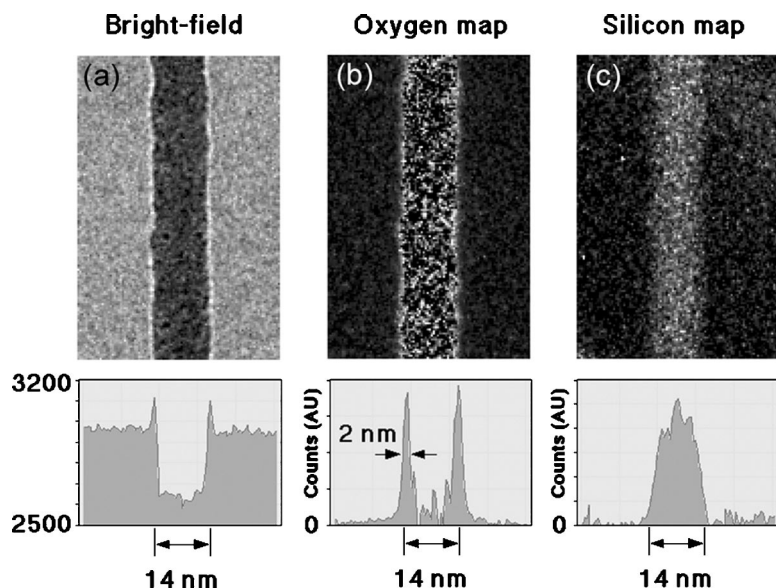


FIG. 6. EELS elemental maps of a portion of a 14-nm-diam SiNW. The bright-field image was acquired slightly under focus (a). Three-window background-subtracted elemental maps were acquired using the oxygen *K* edge (532 eV) (b) and the Si *K* edge (1839 eV) (c) on a 2048 × 2048 pixel CCD camera. The ~2-nm-thick SiO_x sheath corresponds well with the outer amorphous layers seen in the HRTEM analysis (Fig. 4).

grid as a disposable shadow mask. The process conditions were the same as for the samples in Fig. 2. Figure 7(b) shows a nanowire on the same sample pinned by two Pt contacts. The Pt was written by a Ga⁺ focused ion beam from a metal-organic precursor. Deposited metal contacts are used to fix and mark a nanowire. Alternatively, to avoid direct beam exposure, trench markers were set by ion beam milling near individual nanowires. The patterned growth together with pinning and marking of individual SiNWs was used for subsequent Raman spectroscopy analysis.

Raman spectroscopy is one of the main tools to probe carbon nanotubes, being able to assess their chirality, diameter, and their metallic or semiconducting nature.²⁵ As for CNTs, Raman spectroscopy can become a standard technique for nondestructive characterization of SiNWs and a direct probe for quantum confinement effects. Raman scattering is an inelastic process in which incoming photons exchange energy with the crystal vibrational modes. As the photon momentum is very small on the scale of the Brillouin zone, in an infinite crystal light can only interact with phonons having zero momentum, which gives the fundamental selection rule $\mathbf{q} \sim \mathbf{0}$, where \mathbf{q} is the wave vector of the scattered

phonon. The selection rule is relaxed for a finite size domain, due to the Heisenberg uncertainty principle, allowing the participation of phonons near the Brillouin zone center. The phonon uncertainty goes roughly as $\Delta q \sim 1/d$, where d is the grain dimension or NW diameter. As the optic phonon frequency falls away from the zone center in Si, confinement causes lower-frequency phonons to participate.^{26,27} This gives a downshift of the Si peak and an asymmetric broadening. These features can be predicted and calculated by applying the confinement model of Richter *et al.*²⁷ and Campbell and Fauchet²⁶ to a SiNW.

In this article, we only consider the evolution of the main ~520 cm⁻¹ Si first-order Raman peak. Peak positions of ~500–505 cm⁻¹ are reported for wires of ~10–15 nm diameter,^{28–30} and it was claimed that this downshift is due to phonon confinement.^{28–30} However, we calculate that 10–15-nm-diam wires should have a downshift of only ~1 cm⁻¹.^{31,32} The Raman intensity is given by^{26,27}

$$I(\omega) = \int \frac{|C(0, q)|^2}{[\omega - \omega(q)]^2 + (\Gamma_0/2)^2} d^3q. \quad (1)$$

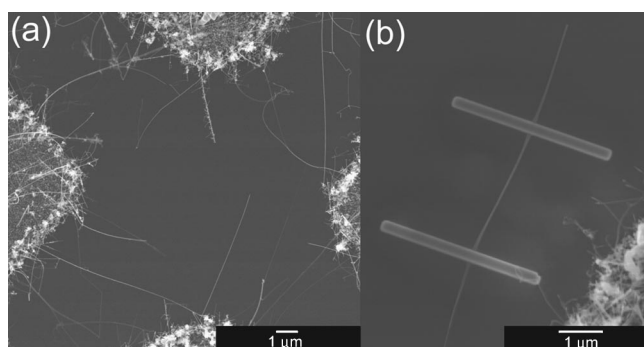


FIG. 7. SEM photograph of selectively grown SiNWs on a Au patterned substrate (a). The pattern allows the pinning of individual nanowires (b). Pt metal contacts were written by a Ga⁺ focused ion beam from a metal-organic precursor.

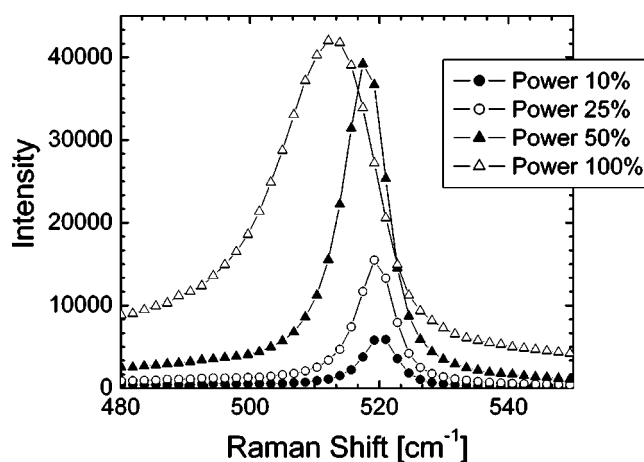


FIG. 8. Raman spectra of SiNW for increasing laser power. The spectra were acquired with a 100× objective and a laser power of 0.02–2.6 mW.

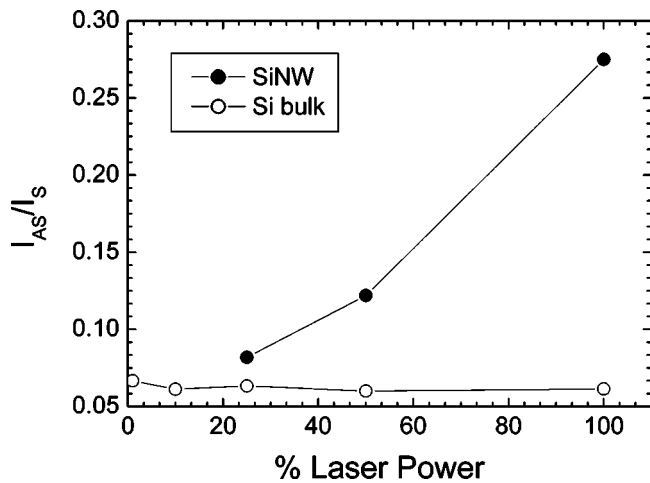


FIG. 9. Anti-Stokes/Stokes intensity ratio as a function of the laser power for a SiNW and bare Si substrate. 100% corresponds to ~ 2.6 mW on the sample.

The integration is over the Brillouin zone. $C(0,q)$ is a Fourier coefficient of the confinement function, and quantifies the $q \neq 0$ phonons participating in the scattering. In our case $|C(0,q)|^2 = \exp(-q^2 d^2 / 16\pi^2)$. We approximate the Si TO dispersion as $\omega(q) = [A + B \cos(q\pi/2)]^{0.5} + D$, with $A = 1.714 \times 10^5 \text{ cm}^{-2}$ and $B = 10^5 \text{ cm}^{-2}$, derived by fitting A and B to the Si TO branch and adjusting D to the bulk reference Si measured with our Raman spectrometer at the same experimental conditions used to measure the SiNWs. Γ_0 is the full width at half maximum (FWHM) of the reference Si. In the case of a quantum dot $d^3 q \propto q^2 dq$, while for a cylindrical nanowire with length \gg diameter $d^3 q \propto q dq$. Indeed, wires are not confined along the axis unlike quantum dots. Thus, the expected Raman frequency and width differ significantly in each case.

Several spectra were acquired at 514.5 nm excitation with a $100\times$ objective and a laser power of 0.02–2.6 mW. A power of a few mW is common in micro-Raman measurements and is comparable to that used in previous papers.^{28–30} Figure 8 shows how, for increasing laser power, the SiNW spectra broaden and downshift significantly. The spectrum taken at ~ 2.6 mW closely resembles in shape and position previously reported data for wires of similar size.^{28–30} However, this is inconsistent with just phonon confinement. Figure 9 shows that the Anti-Stokes/Stokes intensity ratio increases with laser power for a SiNW, whereas it is constant for a bare Si substrate. This ratio increases with local temperature.³³ Figure 9 clearly shows that very low power must be used to avoid local heating of SiNWs. We have improved the standard confinement function (1) by including local heating effects and the resulting anharmonic phonon processes by replacing $\omega(q)$ with $\omega(q, T) = \omega_0(q) + \Delta(T)$ and Γ_0 with $\Gamma_0 + \Gamma(T)$. An analytical expression for $\Delta(T)$ and $\Gamma(T)$ in bulk Si was given by Balkanski *et al.* as a function of four anharmonic constants.³⁴ We calibrated these constants to reproduce the experimental trends on bulk Si on our Raman spectrometer in the 83–700 K range.^{31,32} Figure 10(a) shows a measured low-power spectrum of a SiNW, as compared to crystalline and amorphous Si. The downshift

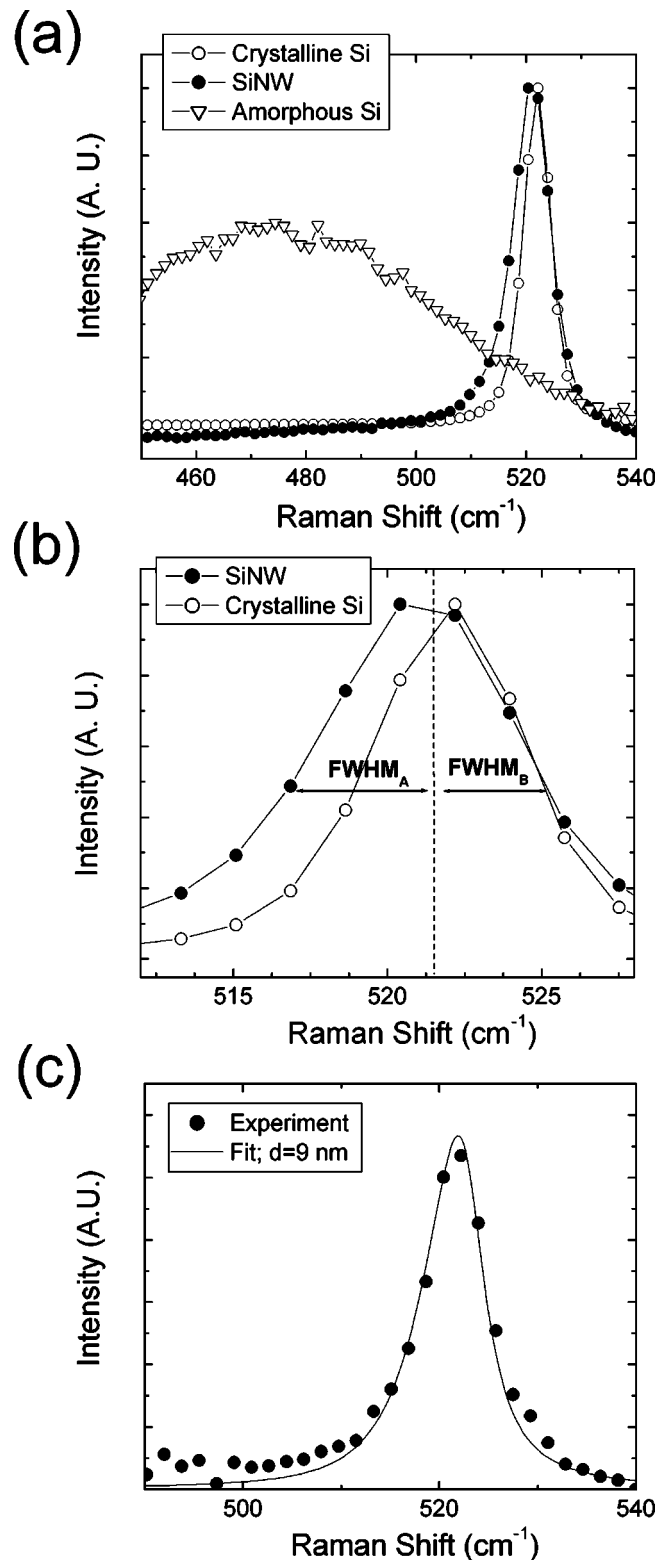


FIG. 10. (a) Low-power Raman spectrum of a SiNW as compared to crystalline and amorphous Si. (b) Downshift and asymmetric broadening ($\text{FWHM}_a > \text{FWHM}_b$) of the SiNW Raman peak with respect to the bulk Si peak. (c) Fit to the measured SiNW spectrum. The fit gives a diameter of ~ 9 nm and a local temperature of ~ 300 K.

($\sim 1 \text{ cm}^{-1}$) and asymmetric broadening of the SiNW peak is evident with respect to the crystalline bulk Si peak [Fig. 10(b)]. Fitting the SiNW spectrum gives a diameter of ~ 9 nm and a local temperature of ~ 300 K [Fig. 10(c)]. This

diameter is in good agreement with the electron microscopy results presented above. This demonstrates confinement effects in as-grown PECVD SiNWs.

IV. GROWTH MODEL ISSUES

The vapor–liquid–solid process is often used to describe thermal growth of metal-catalyzed semiconductor nanowires.^{8,13} Although the individual stages of the VLS reaction can be separated, the detailed processes leading to high-aspect-ratio nanostructures are not well understood. Essentially, the VLS model consists of (1) catalytic decomposition of the source gas on the surface of the metal particles, (2) diffusion of Si from the surface through the catalyst particle or along its surface, and (3) nucleation of the NW and precipitation of Si into the growing structure. The liquid intermediate, namely, the metal–Si eutectic, is not a necessity, as solid catalyst particles can also lead to SiNW growth.²² Therefore, Au could possibly be used below the equilibrium Au/Si eutectic temperature (corrected by particle-size effects³⁵ and pressure influences) especially under plasma conditions.

The effect of the plasma is to preionize the source gas, as well as to provide some local surface heating at low substrate temperatures, which enables an efficient adsorption and diffusion of silicon atoms. Both effects could explain the increased growth rate.

A plasma is a nonisothermal condition, so equilibrium thermodynamic arguments need not always apply. In the VLS mechanism, the supersaturation on the growth interface depends on the diameter. Therefore, the Gibbs–Thomson equation places a lower limit on the diameter of as-grown structures for thermal growth.³⁶ Accordingly, measured growth rates of silicon whiskers were lower for smaller diameter and a critical diameter was found below which growth stops completely.³⁶ In this study, smaller SiNWs show a higher growth rate than thicker structures and we found a continuous diameter distribution rather than a threshold behavior. Following the Gibbs–Thomson equation the lower limit for the wire diameter decreases for increasing silane pressure.⁷ Here, for a pressure range of 0.4–2.4 mbar, we found no significant change in the SiNW diameter distribution. However, increasing pressure increased the nanowire growth rate. An increased silane pressure appears to selectively enhance the catalytical growth process since no tapering due to uncatalytical decomposition of the precursor gas was seen anymore.

The variation of catalyst thickness had no influence on the diameter of crystalline SiNWs. Instead, a thicker Au layer led to the formation of amorphous, worm-like structures of increasing diameter coexisting with the fewer crystalline SiNWs. This is surprising, as in carbon nanotubes the catalyst thickness directly controls the CNT diameter.³⁷ The worm-like features are catalytically grown since Au was always found in the tip matching the diameter of the structure. This indicates that diffusive transport of Si through or on the catalyst particle is fast, supplying Si at a higher rate than the crystallization rate for a given diameter.

Growth directional features of SiNWs are reported for various synthesis methods.¹¹ For low growth rates CVD grown nanowires were seen to adopt the orientation of the Si substrate and grow aligned perpendicular to the surface.⁷ For higher growth rates the growth direction appeared random.⁷ In this study, despite the crystallinity of the as-grown structures, no preferential crystallographic growth direction was found. This may be due to the high growth rate and due to the use of an oxide diffusion barrier screening the substrate orientation.

Compared to carbon nanotubes, SiNWs have a very unstable surface. An oxide layer surrounds all the wires in this study. A hydrogen termination was reported to give a more resistant surface.¹⁹ On the other hand, a wide range of post-growth modifications is possible with SiNWs, such as diameter variation by etching and doping processes. This post-growth tailoring of properties is attractive for many future applications.

V. CONCLUSIONS

Crystalline silicon nanowires have been grown by plasma enhanced chemical vapor deposition at temperatures below 400 °C. The Si nanowires show an uncontaminated silicon core surrounded by a 2-nm-thick oxide sheath. Selective growth on prepatterned substrates enabled pinning and marking of individual nanowires. The as-grown diameters are small enough for the observation of quantum confinement effects by low-power Raman spectroscopy. Plasma activation could allow a further decrease in deposition temperature facilitating direct growth on low-temperature substrates and integration in sensitive nanoelectronic devices.

ACKNOWLEDGMENTS

The authors wish to thank Dae-Joon Kang for the FIB preparation. Two of the authors (A.C.F. and R.E.D.B.) acknowledge the Royal Society for financial support.

¹S. J. Wind, J. Appenzeller, R. Martel, V. Derycke, and P. Avouris, *Appl. Phys. Lett.* **80**, 3817 (2002).

²Y. Cui and C. M. Lieber, *Science* **291**, 851 (2001).

³D. Appell, *Nature (London)* **419**, 553 (2002).

⁴Y. Cui, X. Duan, J. Hu, and C. M. Lieber, *J. Phys. Chem. B* **104**, 5213 (2000).

⁵L. T. Canham, *Appl. Phys. Lett.* **57**, 1046 (1990).

⁶G. D. Sanders and C. Yia-Chung, *Phys. Rev. B* **45**, 9202 (1992).

⁷J. Westwater, D. P. Gosain, S. Tomiya, S. Usui, and H. Ruda, *J. Vac. Sci. Technol. B* **15**, 554 (1997).

⁸A. M. Morales and C. M. Lieber, *Science* **279**, 208 (1998).

⁹D. P. Yu, Z. G. Bai, Y. Ding, Q. L. Hang, H. Z. Zhang, J. J. Wang, Y. H. Zou, W. Qian, G. C. Xiong, H. T. Zhou, and S. Q. Feng, *Appl. Phys. Lett.* **72**, 3458 (1998).

¹⁰J. D. Holmes, K. P. Johnston, R. C. Doty, and B. A. Korgel, *Science* **287**, 71 (2000).

¹¹T. Y. Tan, S. T. Lee, and U. Gosele, *Appl. Phys. A: Mater. Sci. Process.* **74**, 423 (2002).

¹²N. Wang, Y. H. Tang, Y. F. Zhang, C. S. Lee, and S. T. Lee, *Phys. Rev. B* **58**, R16024 (1998).

¹³R. S. Wagner and W. C. Ellis, *Appl. Phys. Lett.* **4**, 89 (1964).

¹⁴R. J. Barsotti, J. E. Fischer, C. H. Lee, J. Mahmood, C. K. W. Adu, and P. C. Eklund, *Appl. Phys. Lett.* **81**, 2866 (2002).

¹⁵T. I. Kamins, R. S. Williams, Y. Chen, Y. L. Chang, and Y. A. Chang, *Appl. Phys. Lett.* **76**, 562 (2000).

- ¹⁶M. K. Sunkara, S. Sharma, R. Miranda, G. Lian, and E. C. Dickey, *Appl. Phys. Lett.* **79**, 1546 (2001).
- ¹⁷B. O. Boskovic, V. Stolojan, R. U. A. Khan, S. Haq, and S. R. P. Silva, *Nat. Mater.* **1**, 165 (2002).
- ¹⁸S. Hofmann, C. Ducati, J. Robertson, and B. Kleinsorge, *Appl. Phys. Lett.* **83**, 135 (2003).
- ¹⁹D. D. D. Ma, C. S. Lee, F. C. K. Au, S. Y. Tong, and S. T. Lee, *Science* **299**, 1874 (2003).
- ²⁰J. F. Geng, B. F. G. Johnson, M. D. R. Thomas, D. S. Shephard, and L. Jiang, *Inorg. Chim. Acta* **330**, 33 (2002).
- ²¹T. I. Kamins, X. Li, and R. S. Williams, *Appl. Phys. Lett.* **82**, 263 (2003).
- ²²T. I. Kamins, R. S. Williams, D. P. Basile, T. Hesjedal, and J. S. Harris, *J. Appl. Phys.* **89**, 1008 (2001).
- ²³K. B. K. Teo, M. Chhowalla, G. A. J. Amaratunga, W. I. Milne, D. G. Hasko, G. Pirio, P. Legagneux, F. Wyczisk, and D. Pribat, *Appl. Phys. Lett.* **79**, 1534 (2001).
- ²⁴C. Yi, L. J. Lauhon, M. S. Gudiksen, W. Jianfang, and C. M. Lieber, *Appl. Phys. Lett.* **78**, 2214 (2001).
- ²⁵A. M. Rao, E. Richter, S. Bandow, B. Chase, P. C. Eklund, K. A. Williams, S. Fang, K. R. Subbaswamy, M. Menon, A. Thess, R. E. Smalley, G. Dresselhaus, and M. S. Dresselhaus, *Science* **275**, 187 (1997).
- ²⁶I. H. Campbell and P. M. Fauchet, *Solid State Commun.* **58**, 739 (1986).
- ²⁷H. Richter, Z. P. Wang, and L. Ley, *Solid State Commun.* **39**, 625 (1981).
- ²⁸S. L. Zhang, W. Ding, Y. Yan, J. Qu, B. Li, L. Y. Li, K. T. Yue, and D. P. Yu, *Appl. Phys. Lett.* **81**, 4446 (2002).
- ²⁹B. Li, D. Yu, and S. L. Zhang, *Phys. Rev. B* **59**, 1645 (1999).
- ³⁰P. C. Eklund, in *Proceedings of the XVIIIth International Conference on Raman Spectroscopy* (Wiley, New York, 2002).
- ³¹A. C. Ferrari, S. Piscanec, S. Hofmann, M. Cantoro, C. Ducati, and J. Robertson, in *Proceedings of IWEPNM 2003* (AIP, Melville, NY, 2003).
- ³²S. Piscanec, M. Cantoro, A. C. Ferrari, A. Zapien, Y. Lifshitz, S. T. Lee, S. Hofmann, and J. Robertson, *Phys. Rev. B* (to be published).
- ³³P. Y. Yu and M. Cardona, *Fundamentals of Semiconductors* (Springer, New York, 1999).
- ³⁴M. Balkanski, R. F. Wallis, and E. Haro, *Phys. Rev. B* **28**, 1928 (1983).
- ³⁵P. Buffat and J. P. Borel, *Phys. Rev. A* **13**, 2287 (1976).
- ³⁶E. I. Givargizov, *J. Cryst. Growth* **31**, 20 (1975).
- ³⁷M. Chhowalla, K. B. K. Teo, C. Ducati, N. L. Rupasinghe, G. A. J. Amaratunga, A. C. Ferrari, D. Roy, J. Robertson, and W. I. Milne, *J. Appl. Phys.* **90**, 5308 (2001).